We are IntechOpen, the world's leading publisher of Open Access books Built by scientists, for scientists

6,900
Open access books available

186,000
International authors and editors

200M
Downloads

154
Countries delivered to

Our authors are among the

TOP 1%
most cited scientists

12.2%
Contributors from top 500 universities

CLARIVATE ANALYTICS
BOOK CITATION INDEX
INDEXED

WEB OF SCIENCE™

Selection of our books indexed in the Book Citation Index
in Web of Science™ Core Collection (BKCI)

Interested in publishing with us?
Contact book.department@intechopen.com

Magnetic Properties of Gadolinium-Doped ZnO Films and Nanostructures

Iman S. Roqan, S. Assa Aravindh and
Singaravelu Venkatesh

Additional information is available at the end of the chapter

Abstract

The magnetic properties of Gd-doped ZnO films and nanostructures are important to the development of next-generation spintronic devices. Here, we elucidate the significant role played by Gd-oxygen-deficiency defects in mediating/inducing ferromagnetic coupling in in situ Gd-doped ZnO thin films deposited at low oxygen pressure by pulsed laser deposition (PLD). Samples deposited at higher oxygen pressures exhibited diamagnetic responses. Vacuum annealing was used on these diamagnetic samples (grown at a relatively high oxygen pressures) to create oxygen-deficiency defects with the aim of demonstrating reproducibility of room-temperature ferromagnetism (RTFM). Samples annealed at oxygen environment exhibited super-paramagnetism and blocking-temperature effects. The samples possessed secondary phases; Gd segregation led to superparamagnetism. Theoretical studies showed a shift of the *4f* level of Gd to the conduction band minimum (CBM) in Gd-doped ZnO nanowires, which led to an overlap with the Fermi level, resulting in strong exchange coupling and consequently RTFM.

Keywords: ZnO, DMS, ferromagnetism, Gd, rare earth

1. Introduction

New generations of electronic devices will likely be developed using spintronics technologies [1]. However, generating reproducible long-range ferromagnetism in wide bandgap (WBG)-diluted magnetic semiconductor (DMS) materials remains a major obstacle to the

fabrication of spintronic devices operating above room temperature [2]. This obstacle has prompted significant research efforts on WBG-DMSs, particularly doped ZnO [3]. Rare earth (RE) dopants have emerged as promising candidates in the search for room-temperature ferromagnetism (RTFM) in ZnO and have been the subject of intense investigations. Doping ZnO with gadolinium (Gd) should produce stronger ferromagnetism compared with doping ZnO with transition metals due to partially filled 4f sublevel [4, 5]. Gd is a RE atom that possesses seven spin-up electrons in partially filled 4f sublevel and one electron in 5d sublevel that are buried deep below fully filled 6s and 5p sublevels. The interesting magnetic properties of RE elements arise from the 4f electrons, which can strongly couple with host s electrons, yielding the possibility of ferromagnetism mediated by carrier electrons. Irrespective of the strong localization of 4f sublevels in RE elements, f-s and f-d magnetic coupling (when f sublevel of Gd^{3+} ion overlaps with s or d band of the host, respectively, allowing exchange coupling) is expected to give rise to strong defect-mediated ferromagnetism in such systems. However, the ferromagnetism of RE dopants remains controversial, owing to the interaction between localized 4f electrons and host electrons [4, 5]. Presently, there is no consensus on the exact exchange mechanism in such WBG-DMSs [6]. The ferromagnetism in ZnO has been attributed to defect-induced [7] or defect-mediated magnetism [8–12]. Furthermore, a density functional theory (DFT) study of Eu-doped ZnO reported ferromagnetic coupling when the RE atoms were in nearest neighbor positions [13]. On the other hand, research on Gd-doped ZnO revealed that ferromagnetic coupling depends on the crystal structure and positions of the dopant atoms in the host matrix, as well as the distance between the RE dopants [14].

Ferromagnetism was observed in Gd-doped ZnO films and nanostructures prepared by different methods [15–20], which can be further improved by annealing [17, 18]. ZnO single crystals implanted with Gd atoms exhibited saturation moments of up to $1.8\mu_B$/Gd [15]. Ferromagnetism has also been observed in nanocrystalline ZnO doped with 3.5% Gd [16]. In addition, Dakhel et al. [20] found that Gd^{3+} ions produce oxygen vacancies in ZnO, which in turn decreases the lattice parameter and increases the tensile stress. Even though magnetic behavior is generally reported in Gd-doped ZnO thin films, these studies failed to obtain long-range FM in Gd-doped ZnO, perhaps due to severe distortion in the crystal as a result of ion implantation damage, to the high Gd dopant concentration (>2 at%), or to the use of lattice-mismatched substrates [15–21]. Paramagnetism has also observed at high concentrations of Gd [21]. This is associated with the precipitation of Gd atoms at higher concentrations, leading to structural degradation. As a consequence, paramagnetism prevails in the sample. On the contrary, Murmu et al. [17, 18] found that at higher concentrations, Gd leads to precipitation in ZnO single crystals, which may also suppress the long-range ferromagnetic order in the material. The structure, doping method, and dopant concentration are therefore crucial factors in determining the magnetic and electronic properties of Gd-doped ZnO. To clarify how Gd-doped ZnO behaves, we report here on experimental and theoretical studies of the magnetic properties of Gd-doped ZnO films and nanostructures.

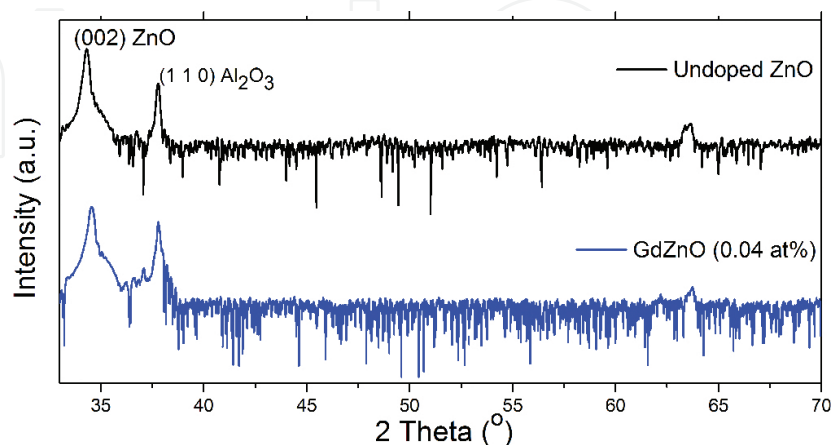# 2. Experimental studies on Gd-doped ZnO thin films

In this section, we describe the ferromagnetic behavior of Gd-doped ZnO thin films as observed experimentally and posited theoretically. We then determine the origin of the ferromagnetism in these materials.

2.1. Sample preparation

All in situ Gd-doped wurtzite ZnO thin films were grown by pulsed laser deposition (PLD) on lattice-matched a-sapphire (Al_2O_3) substrate (0.08% lattice mismatch between [11–21] a-Al_2O_3 and (0 0 0 1) c-ZnO). When the lattice mismatch was minimized, good quality films could be produced as structural defects in which line defects were substantially reduced. The Gd-doped ZnO and Gd targets were synthesized using 99.99% pure ZnO powder mixed with 0.1–2 wt% Gd_2O_3 powder. The films were deposited at different oxygen deposition pressures (P_d) (5–500 mTorr) and at a substrate temperature of 650°C, using a Lambda Physik KrF laser with a wavelength of 248 nm. The details of the target synthesis and PLD conditions are reported in Refs. [22, 23].
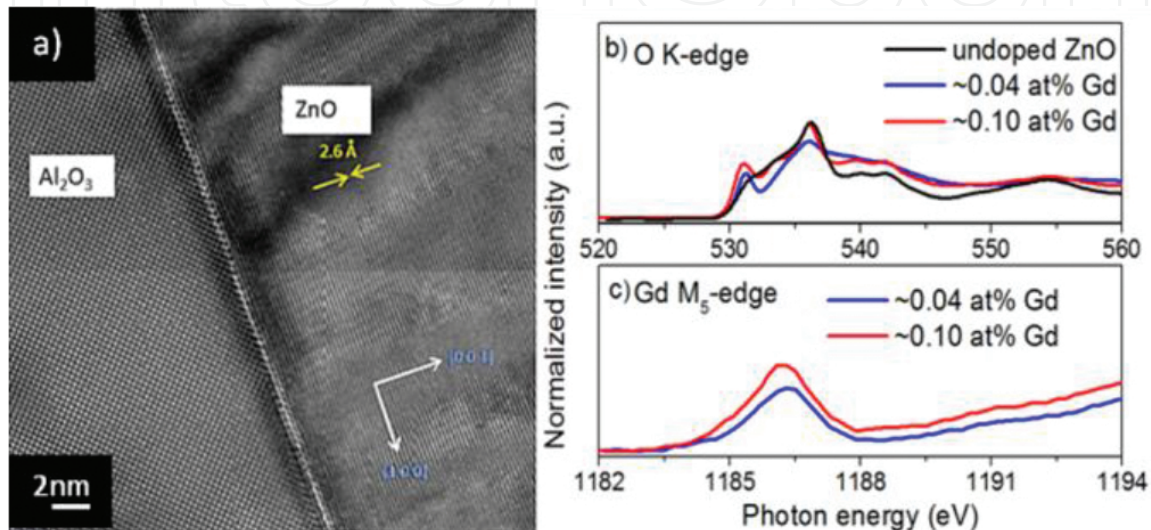
2.2. Structural properties

Understanding the structural properties of the materials is crucial to identifying the origin of their magnetic properties. In this respect, in DMS materials, the film orientation, dopant concentrations, crystal quality, defects, and secondary phase inclusions should be identified clearly. The growth direction, the crystal quality, and the lattice parameters can be studied by X-ray diffraction measurements. A long-range scan (shown in **Figure 1**) of Gd-doped ZnO thin films reveals that they are single crystal and were grown along the c-axis. In the scan shown in **Figure 1**, no secondary or impurity phase could be observed within the resolution limit of the instrument [22]. The lattice parameters were measured using the extended bond method [24] with the (0 0 4) and (1 0 4) planes. The concentration of Gd increases with oxygen pressure (P_d) [25]. The a-parameter increased while the c-parameter decreased with incorporation of Gd

Figure 1. XRD 2θ scans of undoped and Gd-doped ZnO samples showing ZnO growth oriented along the [0 0 0 1] direction (log scale) [22].

compared to without incorporation of Gd. DFT calculations confirmed that Gd-oxygen vacancy (V_O) complexes cause *c*-parameter contraction [25].

We used high-resolution transmission electron microscopy (HR-TEM) to study crystal distortion and to investigate structural defects. The samples did not exhibit any line defects, as shown in **Figure 2**. In addition, no secondary phases were observed near the interface, indicating that the diluted Gd concentration was sufficiently low to prevent the formation of clusters and secondary phases [22].
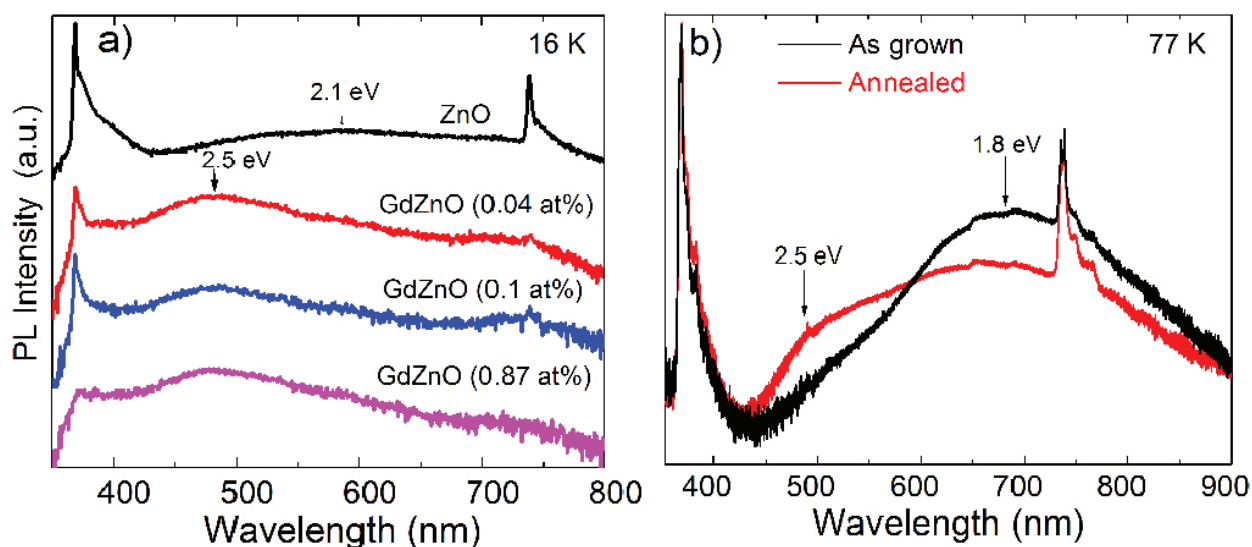

Figure 2. (a) HR-TEM image of a Gd-doped ZnO sample with 0.87 at.% Gd. The image contrast is due to the thickness variation. (b) XAS spectra at the O K-edge. (c) NEXAFS spectra at the Gd M_5-edge after subtracting the background [22].

Materials with secondary phases and segregations are not suitable for practical spintronic applications. Near-edge X-ray absorption fine structure (NEXAFS) spectra can be used to investigate the existence of secondary phases. Because a ZnO matrix cannot be fully polarized and because ferromagnetic signals coming from phase segregation do not contribute to long-range reproducible ferromagnetism, we ran NEXAFS scans to confirm that no secondary phases and segregations were present in the DMS samples. NEXAFS spectra at the O K-edge and Gd $M_{5,4}$-edge revealed the hybridization between Gd and O in Gd-ZnO samples (**Figure 2(b, c)**). The O K-edge spectra shown in **Figure 2(b)** indicate that the two peaks at ~531 eV and ~535 eV are stronger for Gd-doped ZnO compared with those for undoped samples, due to strong O *2p* state hybridization with the Gd 4f and Zn *3d* states [26, 27]. The intensity of these peaks increases as the Gd concentration increases, due to the higher electronegativity of Gd relative to Zn [28, 29]. The Gd valence state measured at the Gd M_5-edge shown in **Figure 2(c)** indicates the 3+ oxidation state of Gd [30, 31]. The intensity variation at 1190 eV increases with increased Gd concentration, which is in good agreement with the O K spectra. The absence of secondary phases and Gd segregation in these films are therefore confirmed by NEXAFS measurements, which is important for elucidating the origin of the magnetic properties of the materials [22].

2.3. Optical properties

The study of optical properties allows the investigation of defects that may affect the magnetic properties of materials. We preformed low-temperature photoluminescence (PL) measurements to study the role of defects. In **Figure 3(a)**, the peak at ~369.1 nm represents the ZnO band edge emission. Moreover, the undoped ZnO spectrum shows an orange-red defect band at 587 nm, which we attributed to oxygen interstitials (O_i) using deep-level transient spectroscopy (DLTS) [32]. The spectra pertaining to the Gd-doped ZnO films grown at low P_d (oxygen-deficiency conditions) show a dominant green PL band at 495 nm (2.50 eV), attributed to V_O [33–36]. Previous research has suggested that this green band in ZnO comes from complex defects, such as defects related to pairs of V_O–Zn vacancies (V_{Zn}) [37] or associated with zinc interstitials (Zn_i) [38] or antisites (O_{Zn}) [39]. A sample grown under rich oxygen conditions ($P_d > 25$ mTorr) shows a dominant red band emission centered at 690 nm as shown in **Figure 3(b)**. We attributed this red band to O_i and V_{Zn} [32, 33]. After a sample was annealed under vacuum conditions to create oxygen vacancies, a significant reduction in the red band was observed, while the spectrum of the vacuum-annealed sample became dominated by the green band (**Figure 3(b)**) [22, 25].
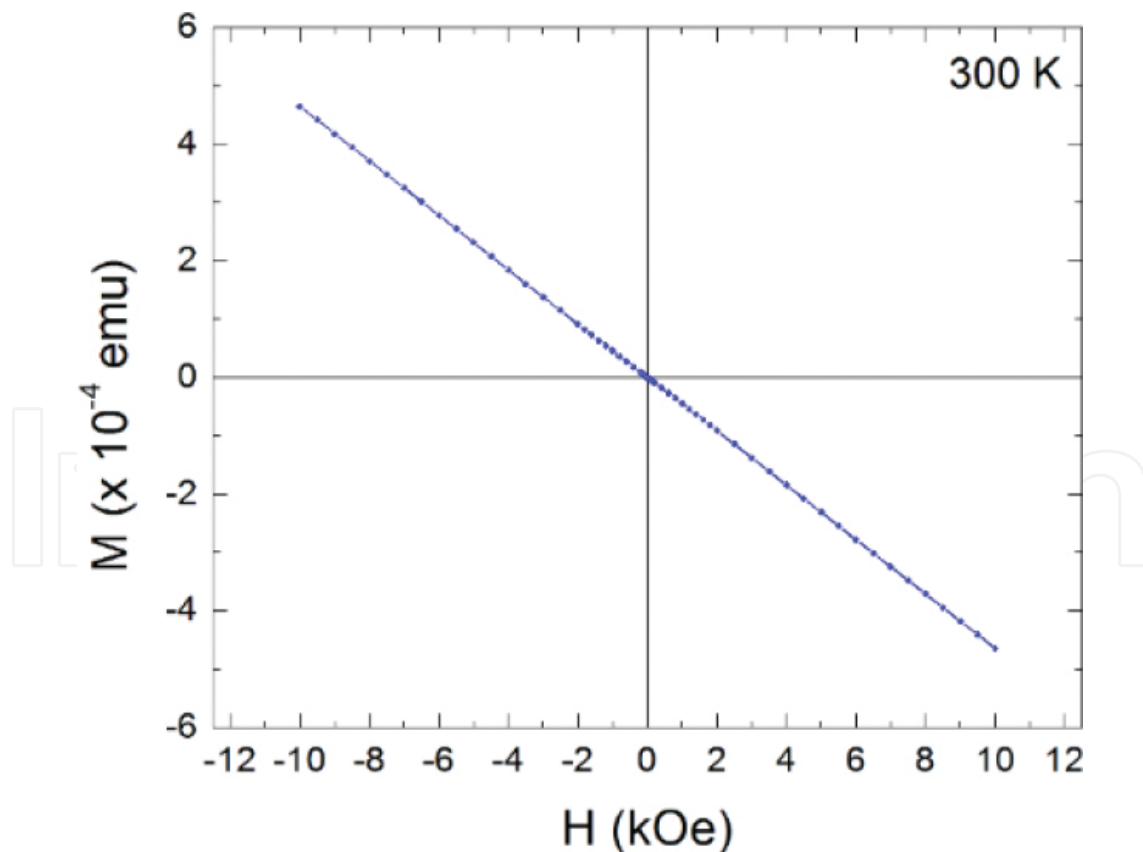

Figure 3. (a) The PL spectra of the samples grown at low P_d and (b) the PL spectra of the sample grown at high P_d before and after vacuum annealing [22].
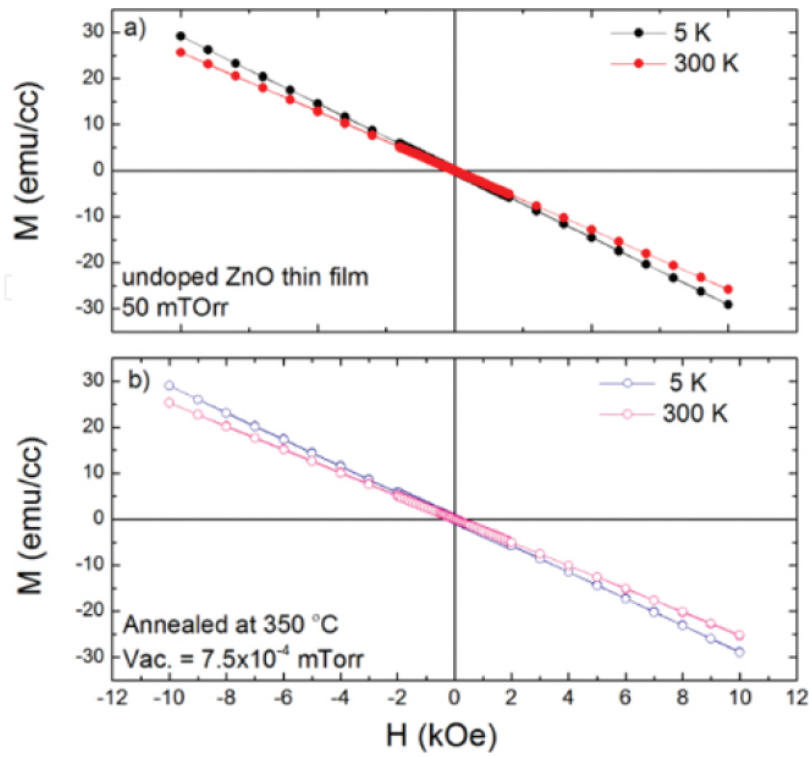
2.4. Magnetic properties

2.4.1. The effect of oxygen deficiency

We measured the magnetization using a superconducting quantum interference device (SQUID) magnetometer (MPMS, Quantum Design, USA) and a SQUID vibrating sample magnetometer (SVSM, Quantum Design, USA). The samples were initially cooled from room temperature to 5 K without application of any magnetic field (zero-field-cooled, ZFC). A field
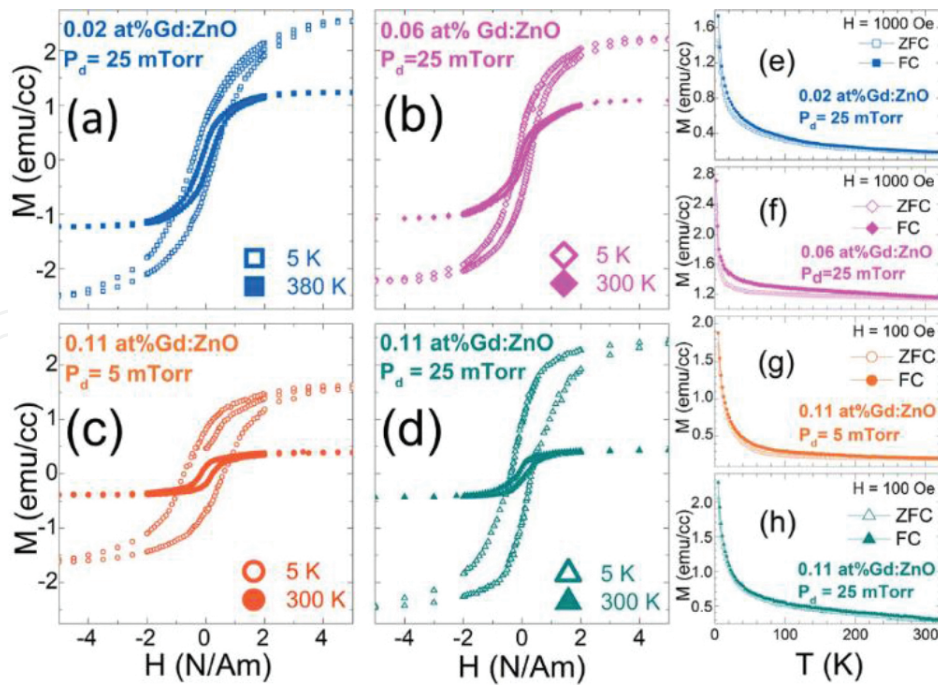
of 100 Oe was then applied and the magnetic data were recorded as a function of temperature as the sample was heated to 300 K and then cooled to 5 K under the same applied field (field-cooled, FC). All undoped ZnO thin films prepared under high or low P_d did not exhibit ferromagnetism before or after vacuum annealing as shown in **Figure 4** and **Figure 5**. All Gd-doped ZnO films deposited at low P_d (≤25 mTorr) exhibited RTFM, as shown in the field strength (H) vs magnetization (M) (H-M) measurements (**Figure 6** and **Figure 7**), whereas samples deposited at higher P_d (with the same concentration of Gd) did not exhibit RTFM (**Figure 8(a)**). **Figure 7** shows H-M loops for samples grown at low P_d (5 mTorr), albeit at different Gd concentrations. All samples investigated produced RTFM responses. Furthermore, nonmagnetic Gd-doped ZnO thin films (deposited at high P_d) became ferromagnetic after vacuum annealing under oxygen-deficiency conditions (**Figure 8(a)**). **Figure 8(b)** shows that the PL defect band related to oxygen deficiency becomes dominant after vacuum annealing. This finding suggests that the introduction of Gd^{3+} ions, together with the presence of certain defects related to oxygen deficiency (such as oxygen vacancies), causes a reproducible long-range ferromagnetic exchange in Gd-doped ZnO thin films. In addition, ferromagnetism is still observed at higher temperatures (380 K), as shown in **Figure 6(a)**, indicating that the Curie temperature (T_C) is above room temperature.

Figure 4. The diamagnetic response of undoped ZnO on a-sapphire prepared by PLD at low oxygen pressure (5 mTorr). The diamagnetic response is shown at 5 K as well.
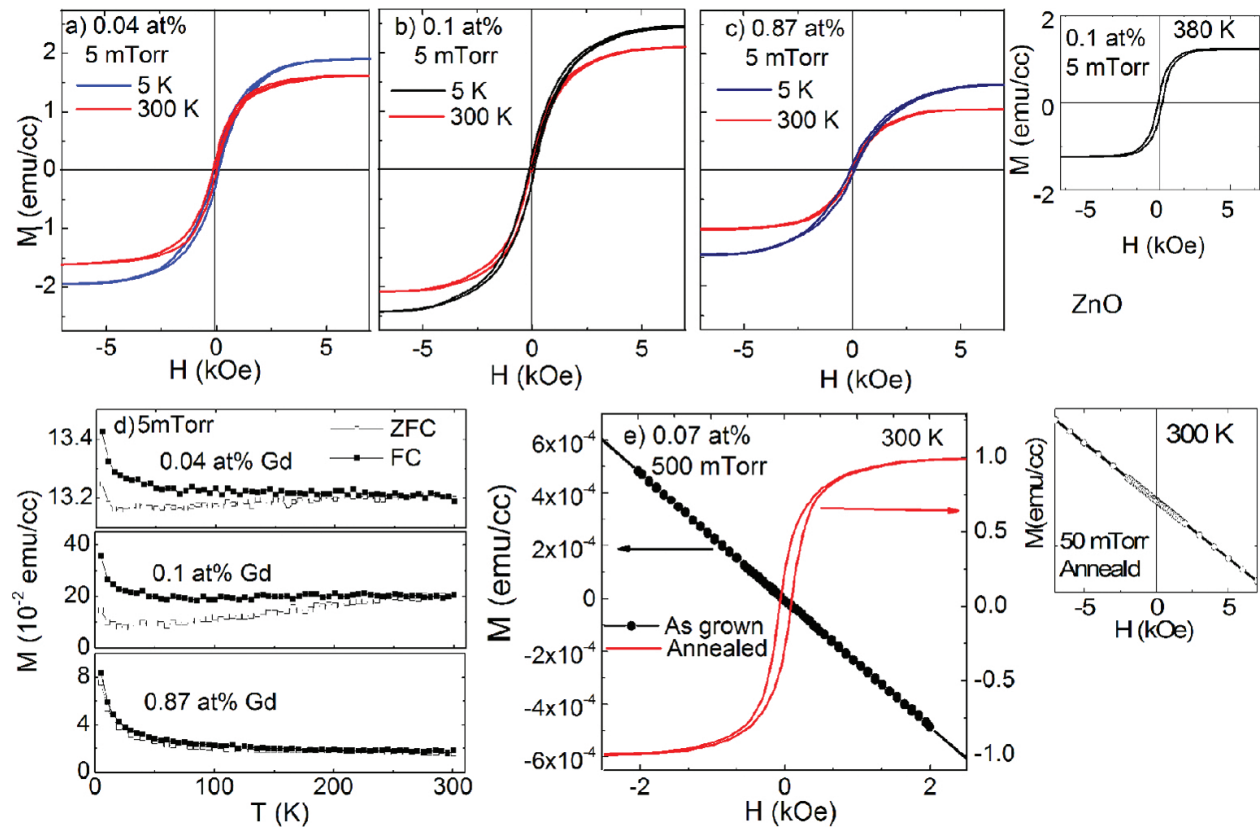
Figure 5. Magnetization measurements of undoped ZnO films deposited at high oxygen pressure (50 mTorr) (a) before and (b) after vacuum annealing under similar conditions of that of Gd-doped ZnO samples.
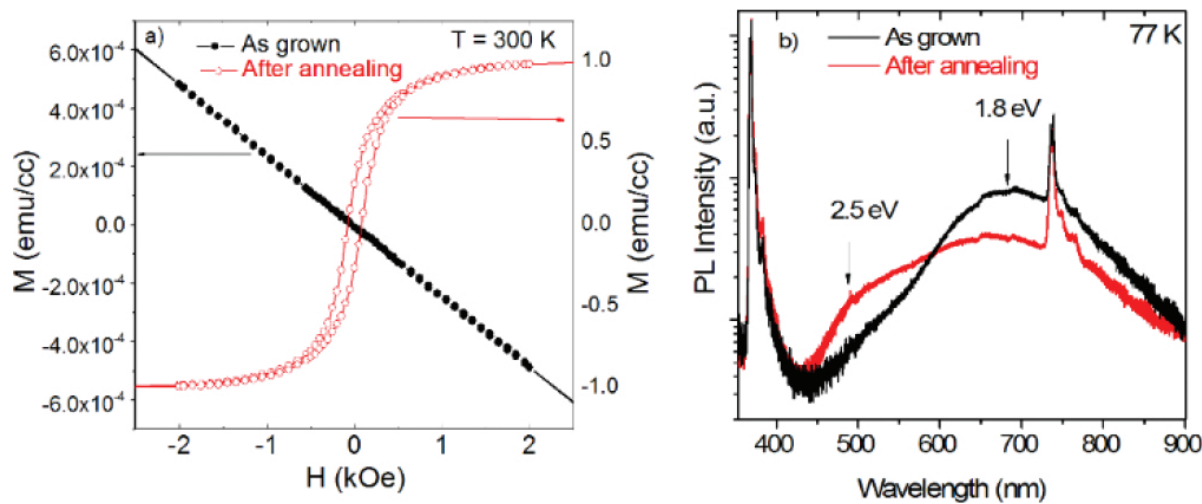

Figure 6. (a)–(d) Typical H-M loops of Gd:ZnO films prepared at $P_d \leq 25$ mTorr. (e)–(f) ZFC and FC for samples shown in (a)–(d), respectively. All measurements were done with H normal to the thin-film plane [23].
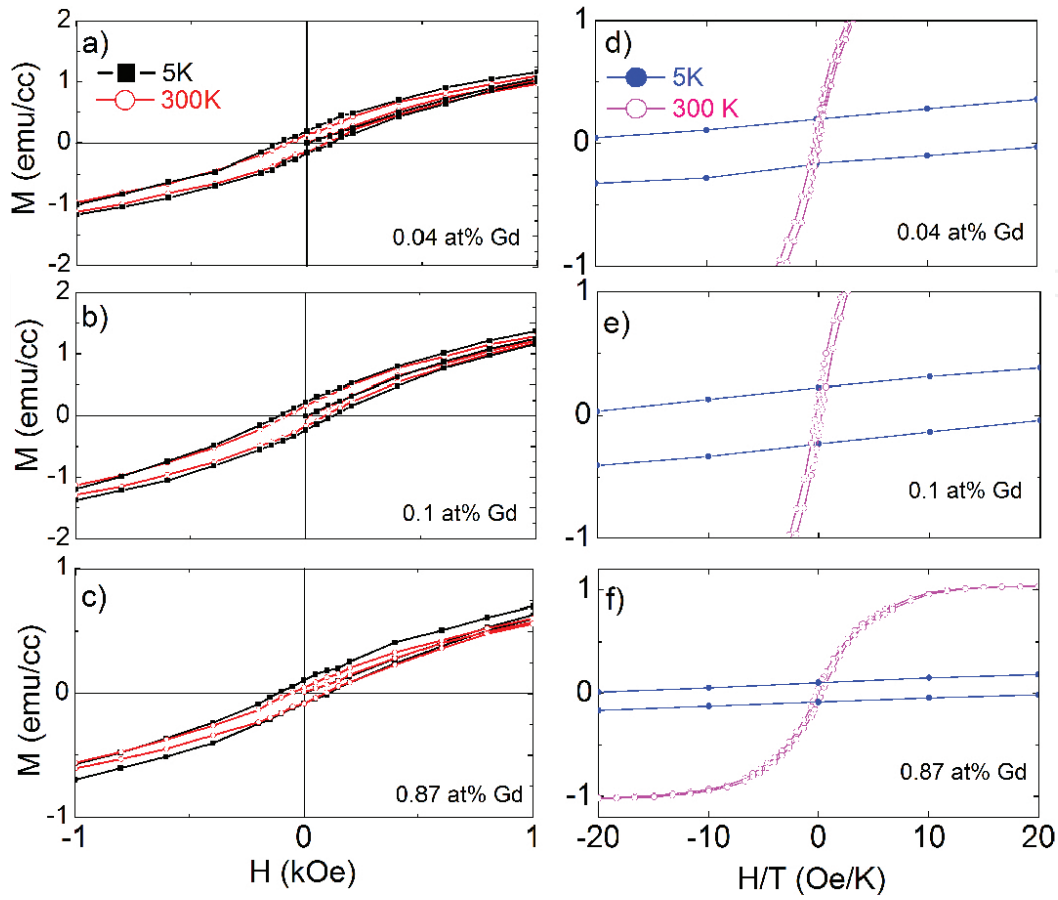
Figure 7. (a)–(c) M-H loops and (d) ZFC-FC magnetization for Gd-doped ZnO samples deposited at 5 mTorr (top inset: M-H loops at high temperature (380 K)) and (e) M-H loops of Gd-doped ZnO samples grown at high P_d and after vacuum annealing (bottom inset: magnetization measurements of undoped ZnO films deposited at high oxygen pressure (50 mTorr) after vacuum annealing) [22].

Figure 8. (a) H-M loops of as-grown Gd-doped ZnO (deposited at high P_d) and after vacuum annealing and (b) their PL spectra. The samples were annealed inside a small glass capsule to avoid any contamination [22].
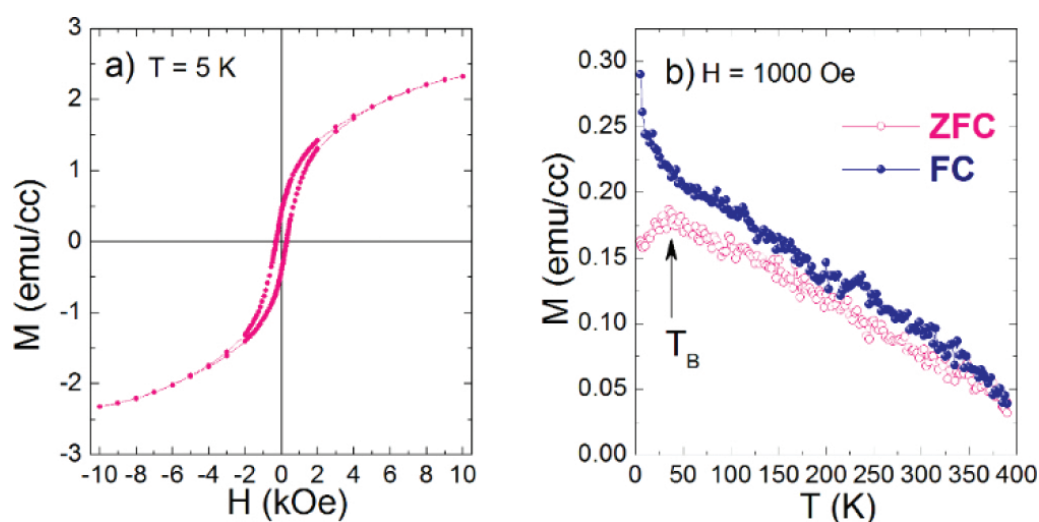
Figure 9. (a)–(c) Nonzero coercivity of H-M loops for Gd-doped ZnO samples deposited at 5 mTorr and (d)–(f) M as a function of H/T for the same Gd-doped ZnO samples, exhibiting ferromagnetic behavior without any superparamagnetic phases [22].

Measurements of the dependence of magnetism on temperature were also conducted. Results are shown in the ZFC and FC curves in **Figure 6** and **Figure 7**. **Figure 6(e–h)** and **Figure 7(d)** show the ZFC-FC curves without magnetic phase transitions or blocking temperatures. Furthermore, nonzero coercivity was observed in both sets of samples at room temperature, as shown in **Figure 6** and **Figure 7**. The magnetism as a function of the field strength/temperature (H/T) in the samples is shown in **Figure 9**, indicating that there is no superimposing universality at 5 K and 300 K, excluding the possibility of superparamagnetism [40]. In addition, the Gd-doped ZnO sample (**Figure 7(a)**) grown with 0.04 at% Gd concentration shows the maximum coercivity (H_C) and the highest magnetic moment of $12.35\mu_B$ per Gd^{3+} ion at 5 K, whereas the sample grown with 0.11 and 0.85 at% Gd concentration shows a magnetic moment of 5.8 (**Figure 7(b)**) and $0.44\mu_B$ per Gd^{3+} ion at 5 K (**Figure 7(c)**). This evidence indicates that no superparamagnetic or spin-glass-like transitions were observed within the temperature range measured in any of the ferromagnetic samples and that RTFM is intrinsic (i.e., it is from the ferromagnetism originating from the polarized ZnO matrix).

To confirm the effect of oxygen defects, a ferromagnetic sample of Gd-doped ZnO (0.08 at% Gd) grown at low P_d (5 mTorr) was annealed at 300°C under flowing oxygen to reduce the

density of the oxygen-deficiency defects in the film. The ferromagnetic signal became very weak and was accompanied by a superparamagnetic signal after annealing as shown in **Figure 10**. The superparamagnetic loop at 5 K suggests a significant reduction in the defect-mediated magnetization. In addition, the blocking temperature (T_B = 37.5 K) is observed in **Figure 10**, indicating the formation of either ferromagnetic and/or antiferromagnetic nanoclusters (cluster size smaller than a magnetic domain) during annealing, which results in the super-paramagnetic behavior of the materials [41, 42]. Murmu et al. [17, 18] reported that annealing Gd-implanted ZnO under a vacuum introduced ferromagnetic and superparamagnetic phases below the blocking temperature, suggesting that this phenomenon is due to ferromagnetic nanoclusters resulting the nonhomogeneous distribution of Gd in the film. A similar transition was observed in antiferromagnetic nanoparticles [43]. In contrast to an antiferro-magnetic bulk material, antiferromagnetic nanoclusters introduced a nonzero magnetic moment because the antiparallel sublattices were characterized by a small angle with respect to the easy magnetic axes. In this case, the spins of the two sublattices were not fully antiparallel with respect to each other, resulting in a net magnetic moment due to the different precession angles [44].
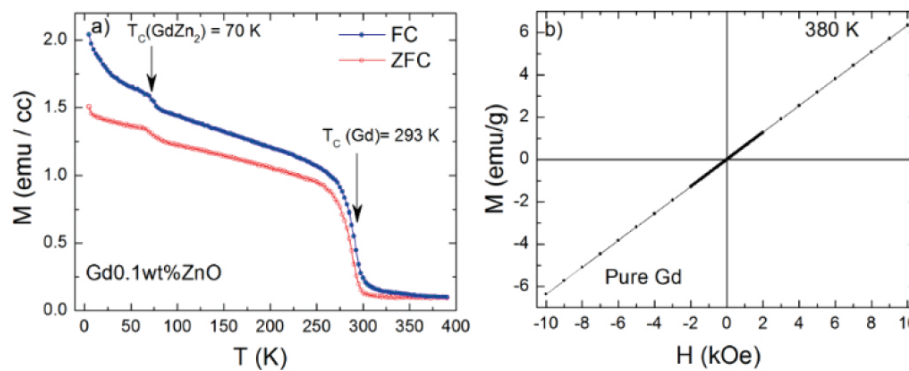

Figure 10. (a) Superparamagnetic behavior after annealing (at 300°C for 5 h in O_2 flow) a ferromagnetic Gd (0.08 at%)-doped ZnO sample. (b) ZFC-FC curves for the sample after annealing.

Extant studies have confirmed that Gd^{3+} ions exhibit magneto-crystalline anisotropy due to the *4f* electron cloud experiencing a tetrahedral crystalline electric field in the lattice and the associated spin splitting [45, 46]. To establish if RTFM is mediated/induced by the Gd-defect complexes, the ferromagnetism would have show magnetic anisotropy. Anisotropic magnet-ization loops were observed in Gd-doped ZnO grown at 25 torr and Gd 0.05 wt% (0.02 at%), indicating a higher magnetic situation when the field (H) was applied parallel to *c*-axis relative to that observed when the field is perpendicular to it. This magnetic anisotropic behavior suggests that the ferromagnetism was due to the Gd-defect complex as RE dopants have strong anisotropy [47]. The exchange interaction is therefore dependent on the Gd concentration. Subramanian et al. [16] observed anisotropy in polycrystalline Gd-doped ZnO [23].
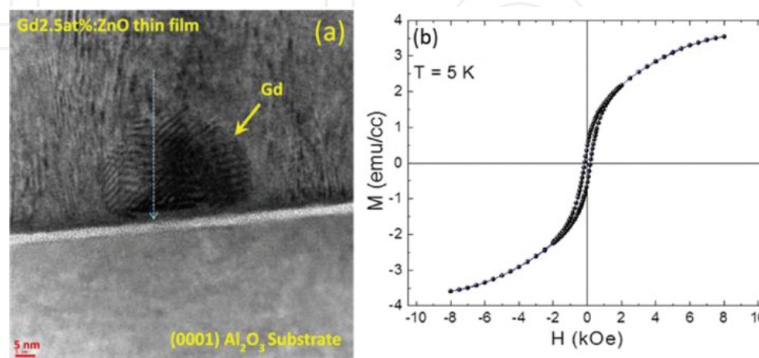
2.4.2. The effect of secondary phases

Finding ferromagnetism in samples annealed at high temperatures (380 K) (described in Sections 2.4.1. and 2.4.2.) suggests that the ferromagnetism does not originate from separation or secondary phases. **Figure 11(a)** shows FC-ZFC curve for a Gd-doped ZnO sample with secondary phases as well as the Curie temperature (T_C) of the Gd clusters. $GdZn_2$ segregation is clearly shown in the curve (T_C at ~70 K as shown in **Figure 11**), whereas the T_C of Gd is very close to room temperature, as shown in **Figure 11(a)**. In addition, paramagnetic signals are observed from Gd metals above room temperature, as shown in **Figure 11(b)**. The other expected phase is Gd_2O_3, which is an antiferromagnetic material.

In highly Gd-doped samples (~2.5 at%) grown at 50 mTorr on c-sapphire substrates, segregation of the secondary phase was observed near the film-substrate interface, as indicated by the HR-TEM results (**Figure 12(a)**). The M-H loop (**Figure 12(b)**) at 5 K is dominated by superparamagnetic behavior, as there is no magnetic saturation. Such behavior was reported by Murmu et al. [19] for (2.5 at%) Gd-implanted ZnO films.

Figure 11. (a) The Curie temperature of other Gd phases. Gd-doped ZnO with a secondary phase and Gd clusters. (b) The pure Gd metal has a paramagnetic response at high temperature (380 K).
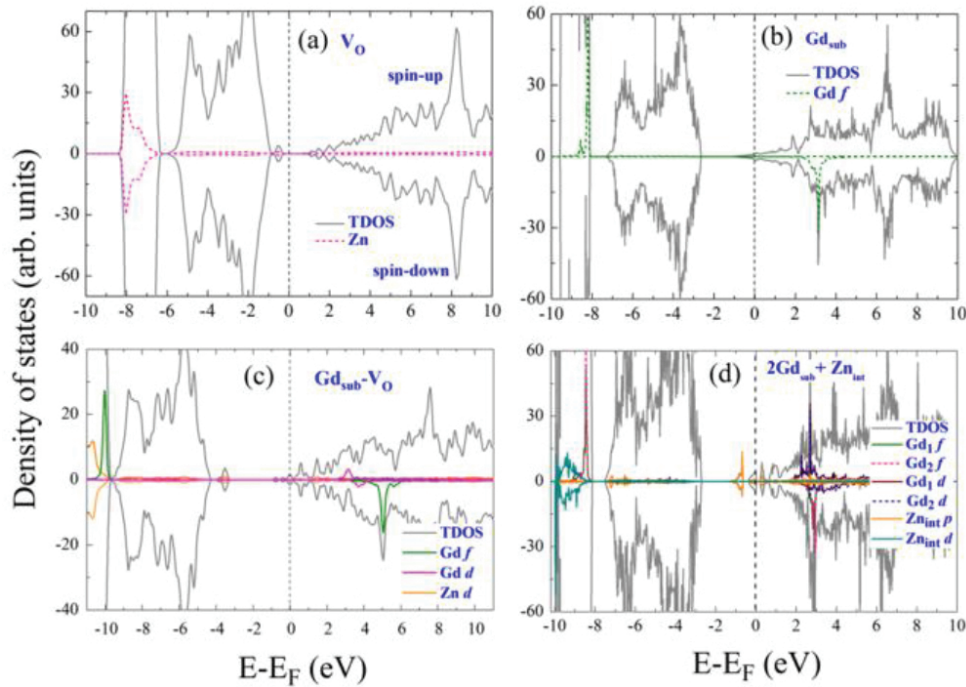

Figure 12. (a) HR-TEM micrograph of Gd (2.5 at%)-doped ZnO deposited on c-sapphire, showing clusters of Gd near the interface. The arrow indicates the line profile from the energy dispersive X-ray (EDX) spectrum showing scanning across the cluster confirming the presence of Gd. (b) M-H loop of the same sample showing a superparamagnetic response.

3. Theoretical studies on Gd-doped ZnO

3.1. The origin of the ferromagnetism in Gd-doped ZnO films

All Gd-doped ZnO samples showed n-type conductivity with about 10^{18} cm^{-3} carrier concentration. RTFM was observed in all samples grown at low P_d. This ferromagnetism can potentially be attributed to Gd-oxygen-deficiency (donor) defects. Theoretical analyses are necessary for in-depth understanding of magnetic interactions.

Figure 13. The DOS of (a) a V_O defect, calculated using the PBE + U; (b) a substitutional Gd (Gd$_{sub}$); (c) Gd + V_O, calculated using hybrid functional HSE06 (α = 0.25 for the Hartree-Fock exchange); and (d) 2Gd$_{sub}$ + Zn$_i$, calculated using PBE + U [22].

The theoretical analysis performed in this work focuses on the effect of the Gd complexes with intrinsic defects that introduce donor electrons [22]. First-principles simulations were performed using the Vienna Ab-initio Simulation Package (VASP) [48, 49] with projector-augmented wave potentials (PAW) and a plane-wave expansion of 400 eV on 2 × 2 × 2 k-meshes for structural relaxation. The exchange and correlations were treated in the Perdew-Burke-Ernzerhof generalized gradient approximation (GGA) and a little higher accuracy for the energy calculation. All configurations were fully relaxed until the forces per atom were less than 0.02 eV/Å. For the localized Zn $3d$ and Gd $4f$ states, Hubbard U correction was taken into account with U$_{eff}$ = 5 eV for Zn $3d$ and 6 eV for Gd $4f$ states. The energy convergence was set to 5 × 10^{-5} eV [22].

Ferromagnetism occurs when the Fermi level (E$_F$) is located near the band edge and overlaps with the impurity level. As a result, it can be partially occupied by the donor electrons and

magnetic exchange coupling can take place [50]. **Figure 13** shows that introducing V_O does not shift the Fermi level to the band edge, which, however, moves above the conduction band minimum (CBM) with the introduction of Gd impurities. However, the presence of Gd dopants in defect-free ZnO is not sufficient to induce exchange coupling, as the magnetic results pertaining to Gd:ZnO reveal predominantly paramagnetic behavior [14]. **Figure 13** shows a 2-Gd complex with V_O and Zn_i, respectively, suggesting three possibilities of magnetic coupling that lead to the observed RTFM in Gd-doped ZnO deposited at different oxygen-deficiency conditions. First, Gd induces FM through *s-f* or *s-d* coupling, which is not possible because the *f* state is far the CBM and does not overlap with the Fermi level, an observation that is in line with our earlier DFT calculations [51]. Second, defect-induced RTFM can be possible in this case if the defect band and the CBM are located near the Fermi level. A shallow donor band located near the Fermi level is created due to the presence of Gd-Zn_i complexes, as shown in **Figure 13**. Therefore, this band may allow ferromagnetic coupling between the *s* state of the host and donor levels, resulting in RTFM. Third, Gd can mediate RTFM, in which case the RTFM will be due to the exchange coupling between the defect states and the host [52]. In this case, the band broadening formed by intrinsic defects is resonant with Gd *f* states producing RTFM [52], as shown in **Figure 13**. Venkatesh et al. [23] showed that the formation of a Gd-oxygen-deficiency defect band located near the Fermi level mediated the ferromagnetism through spin splitting of the defect band [22].

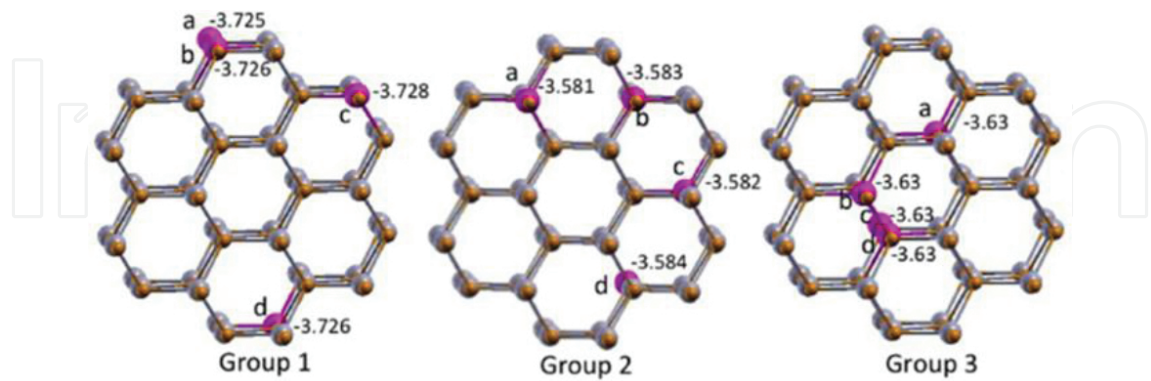## 3.2. The origin of the ferromagnetism in Gd-doped ZnO nanowires

First-principles DFT calculations were carried out within the GGA to elucidate the magnetic phenomena in the Gd-doped ZnO nanowires. A wurtzite ZnO nanowire grown along the [0 0 0 1] direction doped with Gd was considered. The presence of point defects in the nanowire along with the Gd dopant is discussed in the context of magnetic and electronic properties. The possibility of carrier-mediated ferromagnetism originating from the *f-s* coupling was demonstrated using electronic structure analysis [53].

The $Zn_{48}O_{48}$ nanowire was modeled by employing super cell approximation in which a vacuum of 15 Å is created along the X and Y directions and infinite periodicity is maintained along the Z direction. Since a comparison of the results obtained with and without the Hubbard U parameter did not alter the qualitative picture, we adopted the GGA approximation as implemented in the plane-wave-based code VASP [48, 49]. Projected augmented wave (PAW) pseudopotentials were considered with a plane-wave cutoff of 400 eV. A Monkhorst-Pack K grid of 1 × 1 × 8 was used for the Brillouin zone integration. With the abovementioned input settings, we were able to achieve energy and force tolerances of 0.0001 eV and 0.004 eV/Å, respectively.

The formation energy was calculated by incorporating the Gd atoms in all possible non-equivalent sites in the ZnO nanowire encompassing the surface, subsurface, and bulk-like regions (**Figure 14**) using the following equation:

$$E_f = E\left(Zn_{48-m}O_{48}Gd_m\right) - E\left(Zn_{48}O_{48}\right) + n\mu(Zn) - m\mu(Gd), \tag{1}$$

where E and μ denote the total energy and chemical potential (total energy of metallic Zn and Gd), respectively. Here, n represents the number of Zn atoms removed from the supercell and m is the number of Gd atoms replaced by the Zn atoms.

Figure 14. $Zn_{47}O_{48}Gd$ nanowires with all 12 non-equivalent doping sites grouped in to three classes including the surface, subsurface, and bulk-like sites. The formation energy of Gd atoms in each site is also shown (in eV) [53].
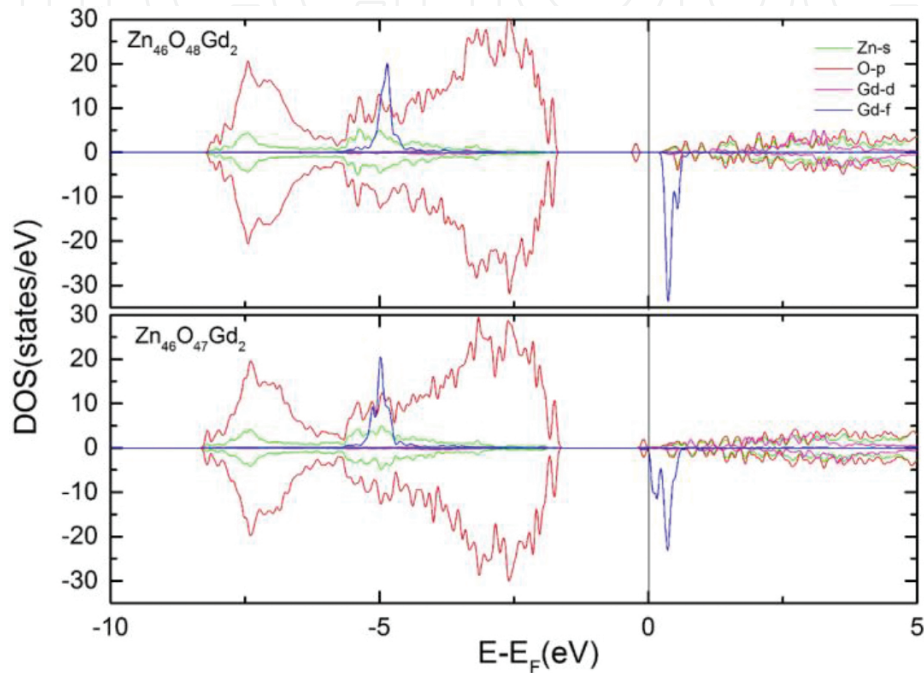
The optimization of a pristine nanowire resulted in a reduction of bond length along the c-axis (1.89 Å), while the ab-plane underwent extension, compared to bulk ZnO (1.99 Å). Substitution of a Gd atom resulted in slight elongation along c-axis, to 2.08 Å, whereas the change within the a-b plane was almost negligible, indicating that the $Zn_{47}O_{48}Gd$ nanowires reached structural stability with minimal lattice distortion. The Gd atoms preferred to occupy the surface sites in agreement with the in situ deposition experiments.

Configuration	ΔE (meV)	$\Delta E(e)$ (meV)	$\Delta E(V_O)$ (meV)
a	4	20	31
b	11	35	96
c	21	57	134
d	9	23	108
e	17	86	200
f	13	21	60
g	9	14	46

Table 1. The difference in total energy (ΔE; meV) between the FM and AFM configurations for the $Zn_{46}O_{48}Gd_2$ nanowires, without vacancies (second column), with electron injection (third column) and with V_O (fourth column).

The energetic preference of the clustering of Gd atoms was analyzed by putting a pair of Gd atoms in the host ZnO matrix and the lowest formation energies for widely separated Gd atoms were obtained. This is an important result indicating that segregation of Gd atoms in ZnO nanowires is unlikely to occur and that the magnetism does not originate from the Gd clusters. Our findings support the homogeneous distribution of RE atoms during implantation in ZnO.

The Gd atoms, when placed in near vicinity, exhibited ferromagnetic exchange coupling in the neutral state with exchange energies (ΔE) as large as 21 meV. The introduction of additional charge to the nanowire by the injection of an electron further enhanced ΔE, indicating that the presence of O vacancies may stabilize ferromagnetic coupling in the nanowire, given that a single O vacancy can release two electrons into the system. The ΔE increased to 200 meV in the presence of O vacancies, supporting the possibility of an increased *f-s* coupling (**Table 1** [53]).

Figure 15. The density of states of Gd-doped ZnO nanowires with and without O vacancies [53].

The density of states (DOS) of Gd-doped ZnO nanowires with and without O vacancies provided further insight into the exchange mechanism. A pristine ZnO nanowire is semiconducting with nonmagnetic characteristics (**Figure 15**) [53]. Doping with Gd atom causes a significant shift of the Fermi level to the conduction band close to the Gd *f* states. The predominant feature observed from DOS is that the majority Gd *f* levels are buried deep inside the valence band and the unoccupied minority states are localized in the vicinity of the Fermi level. With the introduction of V_O, hybridization increases in the vicinity of the Fermi level, mediating the interaction between *s* (from Zn) and the *f* states. In the present context, the ferromagnetic exchange interaction is mediated by the valence electrons provided by the V_O, unlike Zener's *p-d* exchange mechanism in which valence hole states are involved [54]. The double-exchange mechanism is also less likely, as it is based on a physical picture of the d electron hopping between atoms with strong on-site exchange [55]. The shift of the Fermi level towards the conduction band eliminates the possibility of change "*pnf*" to "*p-f*" exchange mediated by the hole states. These findings establish that O vacancies play a key role in stabilizing ferromagnetic exchange in Gd-doped ZnO nanowires.

4. Conclusion

The origin of RTFM in Gd-doped ZnO is intrinsic due to exchange coupling mediated or introduced by a defect band related to the Gd-defect complex. Quantum confinement of the nanowire structure can strengthen the RTFM, as O vacancies play a key role in stabilizing ferromagnetic exchange in Gd-doped ZnO nanowires.

Acknowledgements

Author details

Iman S. Roqan[*], S. Assa Aravindh and Singaravelu Venkatesh

*Address all correspondence to: iman.roqan@kaust.edu.sa

King Abdullah University of Science and Technology (KAUST), Physical Science and Engineering Division, Thuwal, Saudi Arabia

References

[1] G. A. Prinz. Magnetoelectronics. Science. 1998;282:1660–1663.

[2] S. Chambers. Is it really intrinsic ferromagnetism? Nat. Mater. 2010;9:956–957.

[3] P. Sharma, A. Gupta, K. V. Rao, F. J. Owens, R. Sharma, R. Ahuja, J. M. O. Guillen, B. Johansson, G. A. Gehring. Ferromagnetism above room temperature in bulk and transparent thin films of Mn-doped ZnO. Nat. Mater. 2003;2:673–677.

[4] H. Shi, P. Zhang, S. S. Li, J. B. Xia. Magnetic coupling properties of rare-earth metals (Gd, Nd) doped ZnO: first-principles calculations. J. Appl. Phys. 2009;106:023910.

[5]   G. M. Dalpian, S.-H. Wei. Electron-induced stabilization of ferromagnetism in Ga$_{1-x}$Gd$_x$N. Phys. Rev. B. 2005;72:115201.

[6]   P. Dev, P. Zhang. Unconventional magnetism in semiconductors: role of localized acceptor states. Phys. Rev. B. 2010;81:085207.

[7]   X.-L. Li, J.-F. Guo, Z.-Y. Quan, X.-H. Xu, G. A. Gehring. Defects inducing ferromagnetism in carbon-doped ZnO films. IEEE Trans. Magn. 2010;46:1382–1384.

[8]   J. B. Yi, C. C. Lim, G. Z. Xing, H. M. Fan, L. H. Van, S. L. Huang, K. S. Yang, X. L. Huang, X. B. Qin, B. Y. Wang, T. Wu, L. Wang, H. T. Zhang, X. Y. Gao, T. Liu, A. T. S. Wee, Y. P. Feng, J. Ding. Ferromagnetism in dilute magnetic semiconductors through defect engineering: Li-doped ZnO. Phys. Rev. Lett. 2010;104:137201.

[9]   C. D. Pemmaraju, R. Hanafin, T. Archer, H. B. Braun, S. Sanvito. Impurity-ion pair induced high-temperature ferromagnetism in Co-doped ZnO. Phys. Rev. B. 2008;78:054428.

[10] H. Gu, Y. Jiang, Y. Xu, M. Yan. Evidence of the defect-induced ferromagnetism in Na and Co codoped ZnO. Appl. Phys. Lett. 2011;98:012502.

[11] A. Khodorov, A. G. Rolo, E. K. Hlil, J. Ayres de Campos, O. Karzazi, S. Levichev, M. R. Correia, A. Chahboun, M. J. M. Gomes. Effect of oxygen pressure on the structural and magnetic properties of thin Zn0.98Mn0.02O films. Eur. Phys. J. Appl. Phys. 2012;57:10301.

[12] Y. Belghazi, G. Schmerber, S. Colis, J. L. Rehspringer, A. Dinia, A. Berrada. Extrinsic origin of ferromagnetism in ZnO and Zn0.9Co0.1O magnetic semiconductor films prepared by sol–gel technique. Appl. Phys. Lett. 2006;89:122504.

[13] M. H. N. Assadi, Y. Zhang, R. Zheng, S. P. Ringer, S. Li. Structural and electronic properties of Eu- and Pd-doped ZnO. Nanoscale Res. Lett. 2011;6:357.

[14] I. Bantounas, S. Goumri-Said, M. B. Kanoun, A. Manchon, I. Roqan, U. Schwingenschlogl. Ab initio investigation on the magnetic ordering in Gd doped ZnO. J. Appl. Phys. 2011;109:083929.

[15] K. Potzger, S. Zhou, F. Eichhorn, M. Helm, W. Skorupa, A. Mücklich1, J. Fassbender, T. Herrmannsdörfer, A. Bianchi. Ferromagnetic Gd-implanted ZnO single crystals. J. Appl. Phys. 2006;99:063906.

[16] M. Subramanian, P. Thakur, M. Tanemura, T. Hihara, V. Ganesan, T. Soga, K. H. Chae, R. Jayavel, T. Jimbo. Intrinsic ferromagnetism and magnetic anisotropy in Gd-doped ZnO thin films synthesized by pulsed spray pyrolysis method. J. Appl. Phys. 2010;108:053904.

[17] P. P. Murmu, J. Kennedy, B. J. Ruck, G. V. M. Williams, A. Markwitz, S. Rubanov, A. A. Suvorova. Effect of annealing on the structural, electrical and magnetic properties of Gd-implanted ZnO thin films. J. Mater. Sci. 2012;47:1119.

[18] P. P. Murmu, R. J. Mendelsberg, J. Kennedy, D. A. Carder, B. J. Ruck, A. Markwitz, R. J. Reeves, P. Malar, T. Osipowicz. Structural and photoluminescence properties of Gd implanted ZnO single crystal. J. Appl. Phys. 2011;110:033534.

[19] P. P. Murmu, J. Kennedy, G. V. M. Williams, B. J. Ruck, S. Granville, S. V. Chong. Observation of magnetism, low resistivity and magnetoresistance in the near-surface region of Gd implanted ZnO. Appl. Phys. Lett. 2012;101:082408.

[20] A. A. Dakhel, M. El-Hilo. Ferromagnetic nanocrystalline Gd-doped ZnO powder synthesized by coprecipitation. J. Appl. Phys.. 2010;107:123905.

[21] V. Ney, S. Ye, T. Kammermeier, K. Ollefs, F. Wilhelm, A. Rogalev, S. Lebègue, A. L. da Rosa, A. Ney. Structural and magnetic analysis of epitaxial films of Gd-doped ZnO. Phys. Rev. B. 2012;85:235203.

[22] I. S. Roqan, S. Venkatesh, Z. Zhang, S. Hussain, I. Bantounas, J. B. Franklin, T. H. Flemban, B. Zou, J.-S. Lee, U. Schwingenschlogl, P. K. Petrov, M. P. Ryan, N. M. Alford. Obtaining strong ferromagnetism in diluted Gd-doped ZnO thin films through controlled Gd-defect complexes. J. Appl. Phys. 2015;117:073904.

[23] S. Venkatesh, J. B. Franklin, M. P. Ryan, J-S. Lee, H. Ohldag, M. A. McLachlan, N. M. Alford, I. S. Roqan. Defect-band mediated ferromagnetism in Gd-doped ZnO thin films. J. Appl. Phys. 2015;117:013913.

[24] N. Herres, L. Kirste, H. Obloh, K. Kohler, J. Wagner, P. Koidl. X-ray determination of the composition of partially strained group-III nitride layers using the Extended Bond Method. Mater. Sci. Eng. B. 2002;91–92:425–432.

[25] T. H. Flemban, M. C. Sequeira, Z. Zhang, S. Venkatesh, E. Alves, K. Lorenz, I. S. Roqan. Identifying the influence of the intrinsic defects in Gd-doped ZnO thin-films. J. Appl. Phys..2016;119:065301.

[26] L. Armelao, F. Heigl, A. Jurgensen, R. I. R. Blyth, T. Regier, X.-T. Zhou, T. K. Sham. X-ray excited optical luminescence studies of ZnO and Eu-doped ZnO nanostructures. J. Phys. Chem. C. 2007;111:10194.

[27] R. A. Rosenberg, G. K. Shenoy, L. C. Tien, D. Norton, S. Pearton, X. H. Sun, T. K. Sham. Anisotropic X-ray absorption effects in the optical luminescence yield of ZnO nano-structures. Appl. Phys. Lett. 2006;89:093118.

[28] L. A. Grunes, R. D. Leapman, C. N. Wilker, R. Hoffmann, A. B. Kunz. Oxygen K near-edge fine structure: an electron-energy-loss investigation with comparisons to new theory for selected 3d transition-metal oxides. Phys. Rev. B. 1982;25:7157–7173.

[29] J. G. Chen, B. Frühberger, M. L. Colaianni. Near edge X-ray absorption fine structure characterization of compositions and reactivities of transition metal oxides. J. Vac. Sci. Technol. A. 1996;14:1668–1673.

[30] G. Kaindl, G. Kalkowski, W. D. Brewer, B. Perscheid. M-edge X-ray absorption spectroscopy of 4f instabilities in rare earth systems. J. Appl. Phys.. 1984;55:1910–1915.

[31] B. T. Thole, G. van der Laan, J. C. Fuggle, G. A. Sawatzky, R. C. Karnatak, J.-M. Esteva. 3d X-ray-absorption lines and the 3d9 4fn + 1 multiplets of the lanthanides. Phys. Rev. B. 1985;32:5107–5118.

[32] C. H. Ahn, Y. K. Young, C. K. Dong, S. K. Mohanta, H. K. Cho. A comparative analysis of deep level emission in ZnO layers deposited by various methods. J. Appl. Phys. 2009;105:013502.

[33] D. M. Hofmann, D. Pfisterer, J. Sann, B.K. Meyer, R. Tena-Zaera, V. Munoz-Sanjose, T. Frank, G. Pensl. Properties of the oxygen vacancy in ZnO. Appl. Phys. A. 2007;88:147–151.

[34] L. S. Vlasenko, G. D. Watkins. Optical detection of electron paramagnetic resonance in room-temperature electron-irradiated ZnO. Phys. Rev. B. 2005;71:125210.

[35] K. Vanheusden, W. L. Warren, C. H. Seager, D. R. Tallant, J. A. Voigt, B. E. Gnade. Mechanisms behind green photoluminescence in ZnO phosphor powders. J. Appl. Phys. 1996;79:7983–7990.

[36] X. J. Wang, L. S. Vlasenko, S. J. Pearton, W. M. Chen, I. A. Buyanova. Oxygen and zinc vacancies in as-grown ZnO single crystals. J. Phys. D: Appl. Phys.. 2009;42:175411.

[37] J. Ji, L. A. Boatner, F. A. Selim. Donor characterization in ZnO by thermally stimulated luminescence. Appl. Phys. Lett. 2014;105:041102.

[38] N. O. Korsunska, L. V. Borkovska, B. M. Bulakh, L. Y. Khomenkova, V. I. Kushnirenko, I. V. Markevich. The influence of defect drift in external electric field on green luminescence of ZnO single crystals. J. Lumin. 2003;102:733–736.

[39] B. X. Lin, Z. X. Fu, Y. B. Jia.Green luminescent center in undoped zinc oxide films deposited on silicon substrates. Appl. Phys. Lett. 2001;79 :943.

[40] S. Bedanta, W. Kleemann. Supermagnetism. J. Phys. D: Appl. Phys. 2009;42:013001.

[41] J. P. Bucher, D. C. Douglass, L. A. Bloomfield. Magnetic properties of free cobalt clusters. Phys. Rev. Lett. 1991;66:3052–3055.

[42] R. H. Kodama, Salah A. Makhlouf, A. E. Berkowitz. Finite size effects in antiferromagnetic NiO nanoparticles. Phys. Rev. Lett. 1997;79:1393–1396.

[43] S. Mørup, B. R. Hansen. Uniform magnetic excitations in nanoparticles. Phys. Rev. B. 2005;72:024418.

[44] D. C. Douglass, J. P. Bucher, L. A. Bloomfield. Magnetic properties of free cobalt and gadolinium clusters. Phys. Rev. B. 1993;47:12874–12889.

[45] Y. E. Kitaev, P. Tronc. Ferromagnetic and antiferromagnetic ordering in the wurtzite-type diluted magnetic semiconductors. Phys. Sol. State. 2012;54:520–530.

[46] A. Łusakowski. Ground state splitting of S 8 rare earth ions in semiconductors. Phys. Rev. B. 2005;72:094429.

[47] R. Skomski, D. J. Sellmyer. Anisotropy of rare earth magnets. J. Rare Earths. 2009;27:675.

[48] G. Kresse, D. Joubert. Ab initio molecular dynamics for liquid metals. Phys. Rev. B. 1993;47:558

[49] G. Kresse, J. Furthmuller. Efficient iterative schemes for ab initio total-energy calculations using a plane-wave basis set. Phys. Rev. B. 1996;54:11169.

[50] L. Liu, P. Y. Yu, Z. Ma, S. S. Mao. Ferromagnetism in GaN:Gd: a density functional theory study. Phys. Rev. Lett. 2008;100:127203.

[51] I. Bantounas, V. Singaravelu, I. S. Roqan, U. Schwingenschlogl. Structural and magnetic properties of Gd-doped ZnO. J. Mater. Chem. C. 2014;2:10331.

[52] Y. Gohda, A. Oshiyama. Intrinsic ferromagnetism due to cation vacancies in Gd-doped GaN: first-principles calculations. Phys. Rev. B. 2008;78:161201(R).

[53] S. Assa Aravindh, U. Schwingenschoel, I. S. Roqan. Ferromagnetism in Gd doped ZnO nanowires: a first principles study. J. Appl. Phys. 2014;116:233906.

[54] T. Dietl, H. Ohno, F. Matsukura, J. Cibert, D. Ferrand. Zener model description of ferromagnetism in zinc-blende magnetic semiconductors. Science. 2000;287:1091.

[55] P. M. Krstajic, F.M. Peters, A. Ivanov, V. Fleurov, K. Kikoin. Double-exchange mechanisms for Mn-doped III–V ferromagnetic semiconductors. Phys. Rev. B. 2004;70:195215.